Visentin, S., Cannone, G., Doutch, J., Harris, G., Gleghorn, M. L., Clifton, L., Smith, B. O. and Spagnolo, L. (2020) A multi-pronged approach to understanding the form and function of hStaufen protein. *RNA*, 26(3), pp. 265-277. (doi: 10.1261/rna.072595.119)

There may be differences between this version and the published version. You are advised to consult the publisher's version if you wish to cite from it.

http://eprints.gla.ac.uk/205627/

Deposited on 19 December 2019

Enlighten – Research publications by members of the University of Glasgow
http://eprints.gla.ac.uk

Downloaded from rnajournal.cshlp.org on December 20, 2019 - Published by Cold Spring Harbor Laboratory Press

A multi-pronged approach to understanding the form and function of hStaufen protein

Silvia Visentin[1,2,3], Giuseppe Cannone[4,5], James Doutch[3], Gemma Harris[6], Michael L. Gleghorn[7], Luke Clifton[3], Brian O. Smith[1], Laura Spagnolo[1,*]

[1] Institute of Molecular Cell and Systems Biology, University of Glasgow, Glasgow G12 8QQ, UK

[2] Institute of Cell Biology, School of Biological Sciences, University of Edinburgh, Edinburgh, EH9 3JQ, UK

[3] ISIS Pulsed Neutron and Muon Source, Science and Technology Facilities Council (STFC), Rutherford Appleton Laboratory, Didcot, OX11 OQX, UK

[4] Institute of Structural Molecular Biology, School of Biological Sciences, University of Edinburgh, Edinburgh, EH9 3JQ, UK

[5] MRC Laboratory of Molecular Biology, Cambridge CB2 0QH, UK

[6] Research Complex at Harwell, Rutherford Appleton Laboratory, Research Complex at Harwell, Didcot, OX11 0FA, UK

[7] School of Chemistry and Materials Science, College of Science, Rochester Institute of Technology, Rochester, New York 14623, USA

* Corresponding author: Laura.Spagnolo@glasgow.ac.uk

Abstract

Staufen is a dsRNA binding protein involved in many aspects of RNA regulation, such as mRNA transport, Staufen-mediated mRNA decay and the regulation of mRNA translation. It is a modular protein characterized by the presence of conserved consensus amino acid sequences that fold into double-stranded RNA binding domains (RBDs) as well as degenerated RBDs that are instead involved in protein-protein interactions. The variety of biological processes in which Staufen participates in the cell suggests that this protein associates with many diverse RNA targets, some of which have been identified experimentally. Staufen binding mediates the recruitment of effectors via protein-protein and protein-RNA interactions. The structural determinants of a number of these interactions, as well as the structure of full-length Staufen, remain unknown. Here, we present the first solution structure models for full-length hStaufen1[55], showing that its domains are arranged as beads-on-a-string connected by flexible linkers. In analogy with other nucleic acid-binding proteins, this could underpin Stau1 functional plasticity.

Downloaded from rnajournal.cshlp.org on December 20, 2019 - Published by Cold Spring Harbor Laboratory Press

Introduction

Staufen (Stau) is a dsRNA binding protein originally identified in *Drosophila melanogaster*, where it plays an essential role in oocyte development (Schupbach and Wieschaus 1986; St Johnston et al. 1991). It is well conserved from nematodes to humans and, depending on the species, is composed of four or five dsRNA-binding domains (RBDs) (Wickham et al. 1999). In humans, there are two Staufen paralogs: hStau1 and hStau2, each present in several isoforms (Park et al. 2013). Much of our knowledge on human Stau1 is based on the study of isoform hStau1^{55}. hStau1^{55} is associated with 40S and 60S ribosomal subunits and co-localises with the rough endoplasmic reticulum (Marion et al. 1999; Wickham et al. 1999; Luo et al. 2002). hStau1^{55} has also been characterised biochemically in the context of mRNA decay (Kim et al. 2005) and cell cycle control (Boulay et al. 2014). Whilst Stau2 is expressed primarily in the neuromuscular system and is mostly involved in mRNA transport at particular sites of the post-synaptic muscles, Stau1 is ubiquitously expressed (Belanger et al. 2003; Lebeau et al. 2008; Vessey et al. 2008; Ravel-Chapuis et al. 2012; Peredo et al. 2014). Even though Stau1 and Stau2 exhibit different tissue expression patterns, they have been shown to be involved in the same mechanisms of RNA regulation, such as mRNA transport (Martel et al. 2006; Ramasamy et al. 2006; Vessey et al. 2008; Martel et al. 2010; Ravel-Chapuis et al. 2012), Staufen-mediated mRNA decay (SMD) (Kim et al. 2005; Gong et al. 2009; Gong and Maquat 2011; Cho et al. 2012; Baker et al. 2013; Park and Maquat 2013; Kim et al. 2014) and regulation of mRNA translation (Ravel-Chapuis et al. 2012; Bonnet-Magnaval et al. 2016), myogenic differentiation (Ravel-Chapuis et al. 2014), stress granule formation(Ravel-Chapuis et al. 2016), regulation of adipogenesis (Cho et al. 2012; Baker et al. 2013), progression of the cell cycle (Boulay et al. 2014) and cellular differentiation(Gautrey et al. 2005; Gautrey et al. 2008; Kretz 2013; Peredo et al. 2014). They also are central players in virology, functioning in HIV infection by favoring viral RNA (vRNA) encapsidation (Mouland et al. 2000; Chatel-Chaix et al. 2004; Chatel-Chaix et al. 2008; Banerjee et al. 2014), in hepatitis C infection by transporting vRNA to the site of translation, in the replication of cellular DNA (Blackham and McGarvey 2013; Dixit et al. 2016) and as requirements for efficient influenza A virus propagation (de Lucas et al. 2010). The variety of cellular processes in which Stau1 is implicated suggests that it might adopt different binding modes with its diverse RNA targets and that structurally distinct RNA-Stau1

Downloaded from rnajournal.cshlp.org on December 20, 2019 - Published by Cold Spring Harbor Laboratory Press

complexes mediate the recruitment of effectors via protein-protein and/or protein-RNA interactions.

Interactions between Stau1 and its RNA substrates were initially characterised for hStau1^{55}. Multiple copies of hStau1^{55} can bind a single dsRNA. In cells, Stau1 binds intramolecular duplexes within the hARF1 mRNA (Martel et al. 2010). Furthermore, *in vitro*, multiple copies of Stau1 bind to mRNAs containing as many as 250 CUG repeats (Ravel-Chapuis et al. 2012). Additionally, the finding that hStau1^{55} stabilizes imperfectly base-pairings formed between mRNAs and lncRNAs (Gong and Maquat 2011), suggests that multiple hStau1 molecules bind to the same dsRNA. Genome-wide analysis (Furic et al. 2008; Laver et al. 2013) and hiCLIP (RNA hybrid and individual-nucleotide resolution ultraviolet cross-linking and immunoprecipitation) (Fernandez Moya and Kiebler 2015) of Stau-associated mRNAs identified secondary structures that confer binding specificity (Ricci et al. 2014). Nevertheless, what defines a Stau binding site remains unclear (de Lucas et al. 2014).

Stau proteins are characterized by two conserved consensus amino acid sequences that fold into dsRNA binding domains (RBD3 and RBD4); hStau1 contains two other RBDs (RBD2 and RBD5) that are unable to bind RNA and, relative to hStau1, hStau2 has an additional RBD1 and only a partial RBD5(Wickham et al. 1999; Allison et al. 2004),(Buchner et al. 1999; Duchaine et al. 2002; Furic et al. 2008). hStau1 and hStau2 tubulin-binding domains (TBDs), which are involved in mRNA transport on the cytoskeleton, share only 18% identity. Functional activation of a number of dsRNA-binding proteins requires that they self-associate or associate with other dsRNA-binding proteins (Park et al. 2013). A Staufen swapping motif (SSM) has been identified to reside between TBD and RBD5. The SSM is necessary for the homodimeric or heterodimeric interactions between Stau1 and Stau2(Park et al. 2013). This dimerization is critical for SMD (Martel et al. 2010; Gleghorn et al. 2013; Park et al. 2013). The amino terminal α-helix of RBD5 was also identified as the major determinant for protein–protein interaction *in vivo*, intercalating with the two α-helices of the SSM. A recent SEC-MALLS report on purified protein also showed that, in the absence of RNA, SSM-RBD5 promotes dimerization(Lazzaretti et al. 2018). The importance of RBD2 in dimerization is less clear. BRET assays, aimed at the study of hStau1^{55} multimerization, show that RBD2 (amino acids 37–79 of isoform hSTAU1^{55}) interacts with full-length hStau1(Martel et al. 2010). On the other

Downloaded from rnajournal.cshlp.org on December 20, 2019 - Published by Cold Spring Harbor Laboratory Press

hand, recombinant purified hStau1-“RBD”2-RBD3 suggests that the contribution of RBD2 to hStau1^{55} dimerization, while existing, is relatively minor (Martel et al. 2010; Park et al. 2013).

To date, analyses of the three-dimensional structure of Stau proteins have focused on studies of truncated versions of the protein, either in isolation or in complex with short RNA sequences or in complex with truncated versions of interacting proteins. The NMR structure of *Drosophila* RBD3 first confirmed that this construct is organised in the typical α-β-β-β-α□fold (PDB ID: 1STU) (Bycroft et al. 1995). Mouse Stau2 RBD4, in the absence of dsRNA, also showed the α-β-β-β-α □fold (PDB ID: 1UHZ). The structure of human Stau1 SSM-RBD5 solved by X-ray crystallography revealed a domain swapped dimer, which is responsible for mediating hStau1 dimerization (PDB ID: 4DKK) (Gleghorn et al. 2013). The X-ray crystal structure of the complex between Miranda and RBD5 showed two RBD5s symmetrically bound to the Miranda dimeric coiled coil region through their exposed β-sheet faces, revealing a previously unrecognized protein interaction mode for RBDs (PDB ID: 5CFF) (Jia et al. 2015).

The solution structure of *Drosophila melanogaster* Stau RBD3 bound to a 12-bp stem-loop RNA, determined by NMR spectroscopy, revealed the interaction of the canonical α-β-β-β-α □□□D fold with dsRNA (PDB ID: 1EKZ)(Ramos et al. 1999; Ramos et al. 2000). The crystallographic structure of the RBD3-RBD4 construct, bound to dsRNA as a dimer (monomers A and B), shows that the interaction surface with the RNA spans the major groove and the two adjacent minor groove surfaces. Furthermore, RBD3 from monomer B is bound on the opposite side of the RNA molecule, in an antiparallel orientation to RBD3A, whereas density for the second RBD4 is missing (Lazzaretti et al. 2018). Human, *Drosophila*, and *C. elegans* Stau bind dsRNA without apparent sequence specificity *in vitro* (St Johnston et al. 1992; Marion et al. 1999; Wickham et al. 1999; Ramos et al. 2000; LeGendre et al. 2013; Wang et al. 2015). Bono and co-workers recently showed that, in addition to the interactions with the sugar-phosphate backbone previously identified for RBD3(Ramos et al. 2000), both domains of hStau1 directly contact RNA bases in the minor groove of the dsRNA used. Indeed, they also show that specific base recognition is relevant *in vivo* and may therefore contribute to the overall sequence selectivity by Stau, possibly together with additional regions of the protein or with other regulators (Lazzaretti et al. 2018). The macromolecular interaction events that

Downloaded from rnajournal.cshlp.org on December 20, 2019 - Published by Cold Spring Harbor Laboratory Press

happen downstream of Stau RNA binding are still structurally unknown.

We used an integrated structural biology approach, combining homology modelling, small angle X-ray scattering, NMR, and hydrodynamic methods, to characterize the structure of the human full-length Staufen1 protein. To interpret this structure, we also studied an hStau1^{55}_ΔRBD2 truncated variant, individual hStau1^{55} domains, and several tandem multi-domain Stau1 fragments. We confirmed that the deletion of RBD2 influences the oligomeric state of the protein, as well as reporting for the first time its effect on protein solubility. Our data show for the first time that hStau1^{55} adopts an elongated conformation in solution. Furthermore, in the absence of RNA, RBD3 and RBD4 are connected by a linker that is very flexible in solution, and they do not interact with one another.

The reshaping or folding of flexible components in the presence of target nucleic acid in proteins has already been linked to multifunctionality. As an example, DNA and RNA nucleases (Tsutakawa et al. 2014) behave like molecular level transformers that can rebuild themselves by sometimes altering their protein conformations and typically sculpting the nucleic acid to control both their specificity and efficiency functions. We propose that the extreme flexibility and the independent movement of individual domains could also be the basis for the functional plasticity of Stau1 protein: different relative movements of domains on themselves and/or on RNA can create multiple joint recognition surfaces, reshaping itself to elicit diverse RNA metabolism tasks.

Downloaded from rnajournal.cshlp.org on December 20, 2019 - Published by Cold Spring Harbor Laboratory Press

Methods

Cloning of individual and tandem domains for NMR analysis

Individual and tandem hStau1^{55} domains were amplified by PCR from pRSET-B-Stau1^{55} vector (Kim et al. 2005) as described in supplementary Table 1 (Supplementary materials). Purified PCR products and pET28-a were digested with NdeI and HindIIIHF (NEB) for 3 hours at 37°C. Digested vector was purified from 1% agarose gel run in TBE using the MinElute Gel Extraction Kit (QIAGEN), whereas digested inserts were purified using the QIAquick PCR Purification Kit (QIAGEN). Ligations between the vector and the individual inserts (in ratio 1:3) were performed using the Quick Ligation Kit (NEB) for 5 minutes at room temperature (RT). *E.coli* XL1-Blue cells were transformed by the heat-shock method with 2.5 µl of the ligation reactions and plated in LB agar plates containing 50 µg/ml kanamycin. After overnight (o/n), for each of the transformations, 15 ml of LB supplemented with 50 µg/ml kanamycin were inoculated with a single colony and the cultures were grown at 37 °C o/n. Subsequently, plasmid DNA was purified using the Wizard Plus SV Minipreps DNA Purification Systems and sequenced.

Protein overexpression and purification for SAXS, AUC and EM experiments

Recombinant proteins were overexpressed in *E.coli* Rosetta pLysS cells transformed by heat-shock with pRSET-B vectors containing either hStau155_FL(Kim et al. 2005), hStau1^{55}_Δ RBD2 or pET28a containing individual domains (RBD2, RBD3, RBD4, TBD, SSM/RBD5) or tandem domains (RBD2-RBD3, RBD3-RBD4, RBD4-TBD, TBD-SSM/RBD5). Starting cultures were grown in LB medium containing 50 µg/ml ampicillin (for hStau1^{55}_FL and hStau1^{55}_ΔRBD2) or 50 µg/ml kanamycin (for individual and tandem domains) and 34 µg/ml chloramphenicol at 37°C o/n. 1 ml of overnight culture was inoculated in 1L of terrific broth (TB) medium supplemented with antibiotics and cells were grown to an 0.6 OD_{600}. Protein overexpression was induced by adding 0.5 mM IPTG and culturing the cells at 27 °C overnight. Cells were harvested by centrifugation at 5000 rpm on a Beckman AvantiTM J-20 XP centrifuge with JLA 8.1000 rotor for 20 minutes and washed once with phosphate buffered saline (PBS) solution; cell pellets were aliquoted and stocked at -80 °C. Frozen aliquots were thawed and lysed by sonication in 20 ml lysis buffer (25 mM HEPES pH 7.5, 1 M GndCl, 20 mM imidazole, 1% Triton X-100, 400 µl Complete

Downloaded from rnajournal.cshlp.org on December 20, 2019 - Published by Cold Spring Harbor Laboratory Press

EDTA-free protease inhibitors (50X) and 2 μl benzonase) followed by 30 min of incubation on ice. Soluble protein extracts were separated from cell pellets by centrifugation at 15000 rpm for 30 min. 6-His tagged hStau1 proteins were purified by nickel chromatography using HisTrap FF columns (GE Healthcare) equilibrated in washing buffer (25 mM HEPES pH 7.5, 1 M GndCl, 20 mM imidazole). Elution was performed with 20 mM-1 M imidazole gradient. Fractions containing the protein of interest were pooled and concentrated to 10 mg/ml prior to size exclusion chromatography on Superdex200 (hStau1^{55}_FL and hStau1^{55}_ΔRBD2) or Superdex75 (individual and tandem domains) gel filtration columns (GE Healthcare) in buffer A (25 mM HEPES pH 7.5, 100 mM KCl, 10 mM MgCl2, 200 mM L-Arg HCl). Overexpression and purification efficiency were monitored by SDS-PAGE analysis on 12%, 15% and 18% gels stained with SimpleBlue (Life Technologies). Fractions were also analyzed by western blot; the nitrocellulose membrane was incubated o/n at 4 °C with anti-His antibody conjugated with alkaline phosphatase (1:4000) and developed using the SIGMA-FAST™ BCIP/NBT reagent. Size exclusion chromatography and SDS-PAGE analysis for hStau1^{55}_FL and hStau1^{55}_ΔRBD2 are shown in Figure S1, those for individual and tandem domains are shown in Figure S2.

Protein overexpression and purification for NMR analysis

E.coli Rosetta pLysS cells were transformed by heat-shock with pET-28 vectors carrying inserts for hStau1^{55}_FL, hStau1^{55}_ΔRBD2, individual domains (RBD2, RBD3, RBD4, TBD, SSM/RBD5) and tandem domains (RBD2-RBD3, RBD3-RBD4, RBD4-TBD, TBD-SSM/RBD5). Starting cultures were grown as described above and the following day cells were cultured to OD600=2 in TB medium supplemented with antibiotics. Cells were harvested by centrifugation at 5000 rpm on a Beckman AvantiTM J-20 XP centrifuge with JLA 8.1000 rotor for 20 minutes, resuspended in M9 minimal medium (1x M9, 2 mM $MgSO_4$, 0.1 mM $CaCl_2$) and grown for 30 min at 37°C. Successively, the minimal medium was supplemented with 400 μl thiamine [50 mg/ml], filter-sterilized glucose [3 g/L] and filter-sterilized ISOGRO®-15N Powder-Growth Medium [1 g/L]. Protein overexpression was induced by adding 0.5 mM IPTG and culturing the cells at 27 °C overnight. Purification of Staufen proteins was performed as described above, but replacing HEPES with 20 mM potassium

Downloaded from rnajournal.cshlp.org on December 20, 2019 - Published by Cold Spring Harbor Laboratory Press

phosphate buffer pH 7.6 in all buffers used. To prevent formation of disulfide bonds, 2 mM Tris(2-carboxyethyl)phosphine hydrochloride (TCEP) was added to the purified proteins.

Analytical Ultra Centrifugation (AUC)

The experiments were performed at 40,000 rpm, using a Beckman XL-I analytical ultracentrifuge equipped with an An-50Ti rotor. Data were recorded using both absorbance (at 280 nm and 260 nm) and interference optical detection systems. The density and viscosity of the buffer were measured experimentally using a DMA 5000M densitometer equipped with a Lovis 200ME viscometer module. The partial specific volume for the protein was calculated using SEDNTERP from the amino acid sequence. Data were processed using SEDFIT, fitting to the c(s) model. Figures were made using GUSSI(Lebowitz et al. 2002).

SEC-MALS

SEC-MALS experiments were performed using a Superdex 200 10/300 Increase column (GE Healthcare) connected to an AktaPure 25 System (GE Healthcare). The protein sample (100 µL) was loaded onto the gel filtration column and eluted with one column volume (24 mL) of buffer A, at a flow rate of 0.7 ml/min. The eluting protein was monitored using a DAWN HELEOS-II 18-angle light scattering detector (Wyatt Technologies) equipped with a WyattQELS dynamic light scattering module, a U9-M UV/Vis detector (GE Healthcare), and an Optilab T-rEX refractive index monitor (Wyatt Technologies). Data were analysed by using the Astra software (Wyatt Technologies) using a refractive increment value of 0.185 mL/g.

Small Angle X-ray Scattering (SAXS) and Modelling

SAXS data for hStau1^{55}_FL and hStau1^{55}_ΔRBD2 were collected at B21, Diamond Light Source (Harwell, UK). 55 µl of each protein sample (~10 mg/ml) were loaded onto a Superdex200 column (GE Healthcare), controlled by an Agilent HPLC system, coupled to an in-vacuum SAXS flow cell. HPLC-SAXS traces were processed using ScÅtter. High-resolution structures of individual domains were used as rigid bodies and constraints in the model generation. In our analysis, the modelled structures of the individual domains of Staufen1 were obtained using the Phyre2 web portal(Kelley et al. 2015). Human Staufen1 RBD3 was modelled by homology based

Downloaded from rnajournal.cshlp.org on December 20, 2019 - Published by Cold Spring Harbor Laboratory Press

on the NMR structure of *Drosophila melanogaster* Staufen RBD3 (PDB ID: 1EKZ)(Ramos et al. 2000). The structure of human Staufen1 RBD4 was obtained by homology modelling based on the mouse RBD4 (PDB ID: 1UHZ). The structures of SSM and RBD5, were extracted from the structure solved by X-ray crystallography (PDB ID: 4DKK)(Gleghorn et al. 2013) and treated as two separate domains in this analysis, allowing complete inter-domain loop flexibility. To obtain a more complete set of structural information to use as constraints for the interpretation of the SAXS data, the sequences of the 6-His+linker+RBD2 domain of hStau1^{55}_FL, the 6-His+linker of hStau1^{55}_ΔRBD2 and the TBD were modelled using the Phyre2 server(Kelley et al. 2015). The program EOM 2.0(Tria et al. 2015) was used to obtain the models of hStau1^{55}_FL protein and deletion mutants. A pool of 10,000 independent models was generated, based on the sequence of hStau1^{55}_FL, or hStau1^{55}_ΔRBD2, and on constraints we generated by homology modelling. After the creation of the pool of models, EOM (Tria 2015) runs a genetic algorithm that compares the average theoretical scattering intensity from the ensemble of 10,000 conformations with the experimental scattering data and selects the models that best describe the experimental data, taking into account the constraints used as input (in this case, the homology models of individual domains.

SAXS data for individual domains and tandem domains were collected at B21, Diamond Light Source (Harwell, UK). 55 µl of each protein sample (~10 mg/ml) were loaded onto a Superdex75 column (GE Healthcare), controlled by an Agilent HPLC system, coupled to an in-vacuum SAXS flow cell. HPLC-SAXS traces were processed using ScÅtter. Data were analysed using different strategies depending on their flexibility level. Models for individual domains RBD3 and RBD4 were obtained using ScÅtter and DAMMIN and the tandem domain TBD_SSM/RBD5 was modelled using BUNCH (ATSAS). All the other domains, showing higher degree of flexibility, were modelled with EOM, as described above.

NMR spectroscopy

hStau1^{55}_FL, hStau1^{55}_ΔRBD2, individual and tandem domains were studied by NMR spectroscopy. 30 µl of D_2O were added to 570 µl of protein in 20 mM potassium phosphate pH 7.5, 100 mM KCl, 10 mM $MgCl_2$, 200 mM L-Arg HCl, 2mM TCEP at a suitable concentration for NMR experiments (Supplementary Table 2). ^{15}N,^{1}H-TROSY-HSQC spectra(Weigelt 1998) were acquired at 298 K using a Bruker

Downloaded from rnajournal.cshlp.org on December 20, 2019 - Published by Cold Spring Harbor Laboratory Press

AVANCE IIIHD 600 MHz spectrometer equipped with a 5 mm TCI cryoprobe. Data were processed using the Bruker TopSpin software and figures were generated using the CCPN analysis 2.4 software(Vranken et al. 2005).

Downloaded from rnajournal.cshlp.org on December 20, 2019 - Published by Cold Spring Harbor Laboratory Press

Results and Discussion

RBD2 influences both solubility and oligomeric state of Staufen1

Stau proteins were purified to homogeneity by immobilized nickel chromatography followed by size exclusion chromatography. Additive screening to determine conditions that would allow the protein to achieve high concentration and good homogeneity for subsequent structural studies was performed using 10 K MWCO spin-concentrators(Rambo 2017). The addition of L-Arg HCl to the buffer proved necessary for maintaining the solubility of the full-length protein to enable further experiments. Interestingly, the solubility of hStau1^{55}_ΔRBD2 is not affected by the presence (or absence) of L-Arg HCl in the buffer. However, this additive was used for all constructs for consistency with the purification requirements of hStau1^{55}_FL. Size exclusion chromatography (SEC) traces show that the hydrodynamic volumes of hStau1^{55}_FL and of hStau1^{55}_ΔRBD2 (~130-140 kDa) are higher than expected for globular proteins with corresponding molecular weights, suggesting that the two proteins might have an elongated shape or might form homomultimers. The domains organization of hStau1^{55}_FL and hStau1^{55}_ΔRBD2 is shown in Figure 1A. SEC-MALS analysis of hStau1^{55}_FL (Figure 1B) shows the presence of multiple assemblies. In contrast to the recently published SEC profile for hStau1^{63}_FL(Lazzaretti et al. 2018), both SEC profiles for hStau1^{55}_FL and hStau1^{55}_ΔRBD2 described in this study present symmetrical peaks. MALS analysis of the eluting species highlights the different behavior of hStau1^{55}_FL and hStau1^{55}_ΔRBD2. Measurements were performed at three different concentrations (20, 100 and 200 μM). The samples used for this analysis had not been subject to the final SEC purification, hence small amounts of species other than hStau1^{55}_FL and hStau1^{55}_ΔRBD2 were seen to be present. However, the predominant peak in the hStau1^{55}_ΔRBD2 sample had a molecular weight consistent with that of a monomer (Figure 1C). The main SEC peak for hStau1^{55}_FL appears with a molecular weight consistent with a dimer but the high polydispersity seen across the peak suggests that this is an equilibrium species between a monomer and higher order oligomers. This is consistent with the previous observation that RBD2 mediates hStau1^{55}_FL self-association(Martel et al. 2010; Lazzaretti et al. 2018), showing that its presence is fundamental for the formation of a stable oligomer in

Downloaded from rnajournal.cshlp.org on December 20, 2019 - Published by Cold Spring Harbor Laboratory Press

solution. The recent report describing hStau1^{63} did not contain SEC-MALS analysis for the full-length protein(Lazzaretti et al. 2018).

To resolve the oligomeric assemblies of the species eluting in the main SEC peak, we performed analytical ultracentrifugation (AUC) experiments. AUC analysis of the peak fraction from hStau1^{55}_FL SEC (Figure 1D) confirms the co-existence of a number of species with molecular weights consistent with that of the monomer (major species in solution) and higher oligomers. Measurements were performed at three different concentrations (4, 25 and 100 μM). We chose to analyse a wide range of concentrations to address the role of concentration in the oligomeric state of the protein. The number of oligomers increases with increasing sample concentration, and the position of the peaks also shifts to a higher sedimentation co-efficient. Both of these phenomena indicate concentration-dependent self-association equilibrium for hStau1^{55}_FL. On the other hand, both SEC-MALS (Figure 1C) and AUC (Figure 1E) analysis of hStau1^{55}_ΔRBD2 show that the truncated protein is only present in solution as monomer.

Staufen adopts distinct elongated structures in solution

The first indication that Staufen protein and its hStau1^{55}_ΔRBD2 mutant adopt elongated structures in solution is given by their average hydrodynamic volume, which is much higher than expected for the estimated molecular weight of the monomeric protein. This is in agreement with the R_g and D_{max} obtained from SAXS measurements for both the full-length (R_g ensemble= 48.11 Å, D_{max} ensemble= 155.2 Å) and truncated ΔRBD2 (R_g ensemble= 50.26 Å, D_{max} ensemble= 166.96 Å) proteins. The higher R_g and D_{max} for hStau1^{55}_ΔRBD2 can be explained by a higher degree of conformational heterogeneity in the FL protein. Importantly, SAXS shows that both these systems are characterized by a high degree of flexibility, as shown by their Kratky plot in Figure 2. The three-dimensional models of hStau1^{55}_FL protein and of its truncation mutant hStau1^{55}_ΔRBD2 were obtained by combining homology modelling analysis and small angle X-ray scattering data. The models obtained for hStau1^{55}_ΔRBD2 show that the protein adopts a range of conformations (Figure 2), from highly extended to more compact, where RBD3 and RBD5 are in closer proximity. The relative positions of RBD4, TBD and SSM show only minor differences among the models obtained, due to the flexibility of the loops. On the

Downloaded from rnajournal.cshlp.org on December 20, 2019 - Published by Cold Spring Harbor Laboratory Press

other hand, the high level of flexibility of the loops between RBD3 and RBD4 and between SSM and RBD5 seems to be the main factor that contributes to the co-existence of a more distended and a more closed conformation of hStau1^{55}_ΔRBD2. These models show that all the individual domains do not coalesce to form a compact structure. The models obtained for hStau1^{55}_FL, represented in Figure 3, show more inter-domain flexibility, resulting in the presence of elongated, as well as more compact, conformations. The major differences between the co-existing conformations are due to the disordered loops between RBD2 and RBD3, between RBD3 and RBD4 and between RBD4 and TBD. Thanks to the malleability of these linkers, hStau1^{55}_FL seems to be able to transition in solution from more elongated to more closed conformations, but still not globular.

The structural information gathered from the SAXS models for hStau1^{55}_FL and hStau1^{55}_ΔRBD2 were validated using 2D NMR (Figure 4). ^{15}N,^{1}H-TROSY spectra were recorded for individual and tandem domains, as well as for the full-length protein and its truncation mutant ΔRBD2. The large number of peaks in the central area of the spectra of both hStau1^{55}_FL and hStau1^{55}_ΔRBD2 indicates the presence of a large number of amino acids in disordered regions, this agrees well with the presence of long unstructured linkers that confer flexibility on the proteins. Moreover, the similar lineshapes and lack of significant chemical shift perturbations between the spectra recorded for individual and tandem domains (Figures S4 and S5) show that any interactions between adjacent domains are very limited and that each of the domains constituting the tandem constructs tumbles independently in solution, thanks to the intervening linkers flexibility. In addition, it is possible to reconstitute the spectra for hStau1^{55}_FL and hStau1^{55}_ΔRBD2 almost entirely by overlaying those obtained for individual domains, showing that the domains tumble independently in the full-length protein.

Together, our data suggest that hStau1^{55} is an extremely flexible protein and its domains can adopt several positions relative to each other, without inter-domain interactions. Thanks to the flexibility of the linkers, the protein adopts an elongated conformation in solution and its domains behave as beads on a string. Connector regions are crucial players in Staufen allostery and conformational changes, in line

Downloaded from rnajournal.cshlp.org on December 20, 2019 - Published by Cold Spring Harbor Laboratory Press

with recent studies on the role of dynamic linker in the modulation of protein function(Papaleo et al. 2016).

Linker flexibility mediates RBD3 and RBD4 rearrangement

The fitting of a representative subset of SAXS models for individual or tandem domains in the SAXS models of hStau1^{55}_ΔRBD2 and hStau1^{55}_FL is shown in Figure 5 and 6, respectively. The SAXS data and models obtained for individual and tandem domains are shown in Supplementary Figures S6-S14. A representative subset of solution scattering models of individual and tandem domains (Figure 5B) was chosen in order to interpret the domains rearrangement observed in the models corresponding to the different conformations that hStau1^{55}_ΔRBD2 adopts in solution (Figure 5A). From the fitting proposed in Figure 5C, it is possible to observe that in hStau1^{55}_ΔRBD2 the linker connecting RBD3 to RBD4 can be completely or partially distended. SAXS models obtained for the construct RBD3-RBD4 well describe the behavior of these two domains also when they belong to the truncated protein, showing that the presence of TBD and SSM/RBD5 does not have a great impact on RBD3-RBD4 rearrangements. On the contrary, the models obtained for the construct RBD3-RBD4 cannot be used for the interpretation of domains rearrangements in hStau1^{55}_FL (Figure 6A) and a different subset of solution scattering models (Figure 6B) needs to be used in the fitting to describe the conformational changes of the full-length protein (Figure 6C). In fact, the solution models obtained for the tandem domain RBD3-RBD4 (Figure S11) show that a long linker, which is extremely elongated, connects these two domains. On the other hand, our hStau1^{55}_FL models show the coexistence of three main conformations in solution for which it is interesting to notice the relative movement of RBD3 and RBD4 and their closer proximity, possibly in order to elicit the binding of RNA targets (Figure 7). In the more elongated model of the full-length protein (model 1), RBD3 and RBD4 are in a ‘open’ conformation that resembles the one assumed by the tandem domain on its own. However, in the other two models (2 and 3), RBD3 and RBD4 are ‘pulled’ towards each other by conformational changes of the connecting linker, interestingly resembling the recently deposited structure of the hStau1^{63} RBD3-RBD4 construct bound to Arf1 SBS (Lazzaretti et al. 2018) (represented in red and blue in Figure 7).

Downloaded from rnajournal.cshlp.org on December 20, 2019 - Published by Cold Spring Harbor Laboratory Press

Taken together, these data show that not only the presence of RBD2 triggers a spatial reorganization of RBD3 and RBD4, which is indeed mediated by the linker between these last two domains, but also the importance of RBD3-RBD4 relative position and rearrangements on dsRNA binding. Therefore, we propose that these two domains can change mutual orientation depending on the structure of the RNA target, in order to effectively bind different subtracts in distinct biological contexts. Moreover, RBDs that are not involved in the binding of RNAs, such as RBD2 and RBD5, can adopt multiple conformations in the full-length protein, not only to elicit protein dimerization, but also to regulate hStau1 structural plasticity and multi functionality in vivo. All in all, our solution studies demonstrate that Stau protein can adopt several conformations thanks to long linkers that facilitate domains rearrangements, providing a clue on the structural background for the role of Stau in multiple biological pathways. This would be reminiscent of the remodelling of flexible components in the presence of target nucleic acid, which has been seen in other DNA and RNA binding proteins (Tsutakawa et al. 2014) that can change overall shape by altering their protein conformations to switch among their multiple functions.

Downloaded from rnajournal.cshlp.org on December 20, 2019 - Published by Cold Spring Harbor Laboratory Press

Conclusions

Canonical RBDs are composed of an α-β-β-β-α secondary structure that folds in three dimensions to recognize dsRNA. Recently, structural and functional studies of divergent RBDs revealed adaptations that include intra- and/or intermolecular protein interactions, sometimes in the absence of detectable dsRNA-binding ability(Krovat and Jantsch 1996; Gleghorn and Maquat 2014). The number of canonical RBDs per polypeptide is highly variable in RBD-containing proteins, ranging from one to five(Macrae et al. 2006; Barraud and Allain 2012; Thomas and Beal 2017). There is no clear correlation between the number of RBDs and dsRNA binding affinity. Moreover, the extent of the contribution of specific RBDs to RNA substrate specificity is still an open question. Structural information reported on dsRBPs carrying one or more canonical RBD, such as Dicer (Macrae et al.) and ADARs (Barraud and Allain 2012; Thomas and Beal 2017) highlights the importance of neighbouring domains for substrate specificity and enzymatic activity. Conformational flexibility of Dicer protein is also proposed to play a central role in dsRNA recognition and processing (Macrae et al. 2006) and this could be extended to other RBD-containing proteins, such as hStau1. The lack of structural information on this protein, for which to date we only had three-dimensional models of hStau1 truncation mutants, in isolation or in complex with short RNA sequences or truncated protein interactors (Ramos et al. 1999; Ramos et al. 2000; Gleghorn et al. 2013; Gleghorn and Maquat 2014; Jia et al. 2015; Lazzaretti et al. 2018) made its functional understanding particularly challenging. Here, we provided for the first time structural information on the full-length hStau1 protein, using an integrated structural biology approach. Combination of hydrodynamic methods, homology modelling, small angle X-ray scattering and NMR allowed us to show that Stau1 is a highly flexible protein, that recoils in solution from an elongated to a compact conformation in which the domains are in closer proximity but not interacting with each other. In this perspective, we propose that the flexible inter-domain loops possess a regulatory role in hStau1 activity, allowing a high degree of freedom for recognition and binding of diverse RNA and protein targets and for the subsequent involvement of hStau1 in very diverse aspects of RNA metabolism and regulation. Interestingly, post-translational modifications have been identified in loops and linkers regions within hStau1 protein (Rigbolt et al. 2011; Zhou et al. 2013; Guo et al. 2014), which could be involved in the regulation of domains rearrangement or protein-protein interactions.

Downloaded from rnajournal.cshlp.org on December 20, 2019 - Published by Cold Spring Harbor Laboratory Press

As far as the dimerization of hStau1 is concerned, we show that this is dependent on the presence of RBD2 and on protein concentration. Consistently with what has been shown crystallographically, the SSM-RBD5 construct dimerised in solution (Supplementary Figure 2). SAXS experiments show that the full-length protein adopts at least three main conformations in solution, which therefore can explain its ability to bind diverse RNA targets and protein partners. Our data provide the first structural insight into the "Swiss knife" mechanism adopted by the Stau1[55] protein to elicit sometimes contrasting biological functions.

Acknowledgements:

We are grateful to Lynne Maquat for the kind gift of the pRSET-B-Stau1[55] vector(Kim et al. 2005). We acknowledge Eve Hartswood and Amy Whittaker for some initial protein production tests. We are grateful to Drs Robert Rambo, Nathan Cowieson, Nikul Khunti and Katsuaki Inoue (Diamond Light Source, UK) for assistance with data collection at B21, Diamond Light Source, Dr Daniel Myatt (ISIS Pulsed Neutron and Muon Source) for help with the initial scattering experiments and to Dr David Scott for access to biophysical instrumentation at the Research Complex at Harwell. S.V. is supported by an ISIS Neutron Source/University of Edinburgh joint PhD studentship (STFC/SA15). G.C. was supported by a Darwin Trust of Edinburgh PhD studentship.

Downloaded from rnajournal.cshlp.org on December 20, 2019 - Published by Cold Spring Harbor Laboratory Press

Bibliography

Allison R, Czaplinski K, Git A, Adegbenro E, Stennard F, Houliston E, Standart N. 2004. Two distinct Staufen isoforms in Xenopus are vegetally localized during oogenesis. *RNA* **10**: 1751-1763.

Baker KS, Chow EJ, Goodman PJ, Leisenring WM, Dietz AC, Perkins JL, Chow L, Sinaiko A, Moran A, Petryk A et al. 2013. Impact of treatment exposures on cardiovascular risk and insulin resistance in childhood cancer survivors. *Cancer Epidemiol Biomarkers Prev* **22**: 1954-1963.

Banerjee A, Benjamin R, Balakrishnan K, Ghosh P, Banerjee S. 2014. Human protein Staufen-2 promotes HIV-1 proliferation by positively regulating RNA export activity of viral protein Rev. *Retrovirology* **11**: 18.

Barraud P, Allain FH. 2012. ADAR proteins: double-stranded RNA and Z-DNA binding domains. *Curr Top Microbiol Immunol* **353**: 35-60.

Belanger G, Stocksley MA, Vandromme M, Schaeffer L, Furic L, DesGroseillers L, Jasmin BJ. 2003. Localization of the RNA-binding proteins Staufen1 and Staufen2 at the mammalian neuromuscular junction. *Journal of neurochemistry* **86**: 669-677.

Blackham SL, McGarvey MJ. 2013. A host cell RNA-binding protein, Staufen1, has a role in hepatitis C virus replication before virus assembly. *J Gen Virol* **94**: 2429-2436.

Bonnet-Magnaval F, Philippe C, Van Den Berghe L, Prats H, Touriol C, Lacazette E. 2016. Hypoxia and ER stress promote Staufen1 expression through an alternative translation mechanism. *Biochemical and biophysical research communications* **479**: 365-371.

Boulay K, Ghram M, Viranaicken W, Trepanier V, Mollet S, Frechina C, DesGroseillers L. 2014. Cell cycle-dependent regulation of the RNA-binding protein Staufen1. *Nucleic acids research* **42**: 7867-7883.

Buchner G, Bassi MT, Andolfi G, Ballabio A, Franco B. 1999. Identification of a novel homolog of the Drosophila staufen protein in the chromosome 8q13-q21.1 region. *Genomics* **62**: 113-118.

Bycroft M, Grunert S, Murzin AG, Proctor M, St Johnston D. 1995. NMR solution structure of a dsRNA binding domain from Drosophila staufen protein reveals homology to the N-terminal domain of ribosomal protein S5. *The EMBO journal* **14**: 3563-3571.

Chatel-Chaix L, Boulay K, Mouland AJ, Desgroseillers L. 2008. The host protein Staufen1 interacts with the Pr55Gag zinc fingers and regulates HIV-1 assembly via its N-terminus. *Retrovirology* **5**: 41.

Chatel-Chaix L, Clement JF, Martel C, Beriault V, Gatignol A, DesGroseillers L, Mouland AJ. 2004. Identification of Staufen in the human immunodeficiency virus type 1 Gag ribonucleoprotein complex and a role in generating infectious viral particles. *Molecular and cellular biology* **24**: 2637-2648.

Cho H, Kim KM, Han S, Choe J, Park SG, Choi SS, Kim YK. 2012. Staufen1-mediated mRNA decay functions in adipogenesis. *Molecular cell* **46**: 495-506.

de Lucas S, Oliveros JC, Chagoyen M, Ortin J. 2014. Functional signature for the recognition of specific target mRNAs by human Staufen1 protein. *Nucleic acids research* **42**: 4516-4526.

de Lucas S, Peredo J, Marion RM, Sanchez C, Ortin J. 2010. Human Staufen1 protein interacts with influenza virus ribonucleoproteins and is required for efficient virus multiplication. *Journal of virology* **84**: 7603-7612.

Downloaded from rnajournal.cshlp.org on December 20, 2019 - Published by Cold Spring Harbor Laboratory Press

Dixit U, Pandey AK, Mishra P, Sengupta A, Pandey VN. 2016. Staufen1 promotes HCV replication by inhibiting protein kinase R and transporting viral RNA to the site of translation and replication in the cells. *Nucleic acids research* **44**: 5271-5287.

Duchaine TF, Hemraj I, Furic L, Deitinghoff A, Kiebler MA, DesGroseillers L. 2002. Staufen2 isoforms localize to the somatodendritic domain of neurons and interact with different organelles. *Journal of cell science* **115**: 3285-3295.

Fernandez Moya SM, Kiebler MA. 2015. CLIPing Staufen to secondary RNA structures: size and location matter! *BioEssays : news and reviews in molecular, cellular and developmental biology* **37**: 1062-1066.

Furic L, Maher-Laporte M, DesGroseillers L. 2008. A genome-wide approach identifies distinct but overlapping subsets of cellular mRNAs associated with Staufen1- and Staufen2-containing ribonucleoprotein complexes. *RNA* **14**: 324-335.

Gautrey H, McConnell J, Hall J, Hesketh J. 2005. Polarised distribution of the RNA-binding protein Staufen in differentiated intestinal epithelial cells. *FEBS letters* **579**: 2226-2230.

Gautrey H, McConnell J, Lako M, Hall J, Hesketh J. 2008. Staufen1 is expressed in preimplantation mouse embryos and is required for embryonic stem cell differentiation. *Biochimica et biophysica acta* **1783**: 1935-1942.

Gleghorn ML, Gong C, Kielkopf CL, Maquat LE. 2013. Staufen1 dimerizes through a conserved motif and a degenerate dsRNA-binding domain to promote mRNA decay. *Nat Struct Mol Biol* **20**: 515-524.

Gleghorn ML, Maquat LE. 2014. 'Black sheep' that don't leave the double-stranded RNA-binding domain fold. *Trends Biochem Sci* **39**: 328-340.

Gong C, Kim YK, Woeller CF, Tang Y, Maquat LE. 2009. SMD and NMD are competitive pathways that contribute to myogenesis: effects on PAX3 and myogenin mRNAs. *Genes & development* **23**: 54-66.

Gong C, Maquat LE. 2011. lncRNAs transactivate STAU1-mediated mRNA decay by duplexing with 3' UTRs via Alu elements. *Nature* **470**: 284-288.

Guo A, Gu H, Zhou J, Mulhern D, Wang Y, Lee KA, Yang V, Aguiar M, Kornhauser J, Jia X et al. 2014. Immunoaffinity enrichment and mass spectrometry analysis of protein methylation. *Mol Cell Proteomics* **13**: 372-387.

Jia M, Shan Z, Yang Y, Liu C, Li J, Luo ZG, Zhang M, Cai Y, Wen W, Wang W. 2015. The structural basis of Miranda-mediated Staufen localization during Drosophila neuroblast asymmetric division. *Nature communications* **6**: 8381.

Kelley LA, Mezulis S, Yates CM, Wass MN, Sternberg MJ. 2015. The Phyre2 web portal for protein modeling, prediction and analysis. *Nat Protoc* **10**: 845-858.

Kim MY, Park J, Lee JJ, Ha DH, Kim J, Kim CG, Hwang J, Kim CG. 2014. Staufen1-mediated mRNA decay induces Requiem mRNA decay through binding of Staufen1 to the Requiem 3'UTR. *Nucleic acids research* **42**: 6999-7011.

Kim YK, Furic L, Desgroseillers L, Maquat LE. 2005. Mammalian Staufen1 recruits Upf1 to specific mRNA 3'UTRs so as to elicit mRNA decay. *Cell* **120**: 195-208.

Kretz M. 2013. TINCR, staufen1, and cellular differentiation. *RNA biology* **10**: 1597-1601.

Krovat BC, Jantsch MF. 1996. Comparative mutational analysis of the double-stranded RNA binding domains of Xenopus laevis RNA-binding protein A. *The Journal of biological chemistry* **271**: 28112-28119.

Downloaded from rnajournal.cshlp.org on December 20, 2019 - Published by Cold Spring Harbor Laboratory Press

Laver JD, Li X, Ancevicius K, Westwood JT, Smibert CA, Morris QD, Lipshitz HD. 2013. Genome-wide analysis of Staufen-associated mRNAs identifies secondary structures that confer target specificity. *Nucleic acids research* **41**: 9438-9460.

Lazzaretti D, Bandholz-Cajamarca L, Emmerich C, Schaaf K, Basquin C, Irion U, Bono F. 2018. The crystal structure of Staufen1 in complex with a physiological RNA sheds light on substrate selectivity. *Life Sci Alliance* **1**: e201800187.

Lebeau G, Maher-Laporte M, Topolnik L, Laurent CE, Sossin W, Desgroseillers L, Lacaille JC. 2008. Staufen1 regulation of protein synthesis-dependent long-term potentiation and synaptic function in hippocampal pyramidal cells. *Molecular and cellular biology* **28**: 2896-2907.

Lebowitz J, Lewis MS, Schuck P. 2002. Modern analytical ultracentrifugation in protein science: a tutorial review. *Protein science : a publication of the Protein Society* **11**: 2067-2079.

LeGendre JB, Campbell ZT, Kroll-Conner P, Anderson P, Kimble J, Wickens M. 2013. RNA targets and specificity of Staufen, a double-stranded RNA-binding protein in Caenorhabditis elegans. *The Journal of biological chemistry* **288**: 2532-2545.

Luo M, Duchaine TF, DesGroseillers L. 2002. Molecular mapping of the determinants involved in human Staufen-ribosome association. *The Biochemical journal* **365**: 817-824.

Macrae IJ, Li F, Zhou K, Cande WZ, Doudna JA. 2006. Structure of Dicer and mechanistic implications for RNAi. *Cold Spring Harb Symp Quant Biol* **71**: 73-80.

Marion RM, Fortes P, Beloso A, Dotti C, Ortin J. 1999. A human sequence homologue of Staufen is an RNA-binding protein that is associated with polysomes and localizes to the rough endoplasmic reticulum. *Molecular and cellular biology* **19**: 2212-2219.

Martel C, Dugre-Brisson S, Boulay K, Breton B, Lapointe G, Armando S, Trepanier V, Duchaine T, Bouvier M, Desgroseillers L. 2010. Multimerization of Staufen1 in live cells. *RNA* **16**: 585-597.

Martel C, Macchi P, Furic L, Kiebler MA, Desgroseillers L. 2006. Staufen1 is imported into the nucleolus via a bipartite nuclear localization signal and several modulatory determinants. *The Biochemical journal* **393**: 245-254.

Mouland AJ, Mercier J, Luo M, Bernier L, DesGroseillers L, Cohen EA. 2000. The double-stranded RNA-binding protein Staufen is incorporated in human immunodeficiency virus type 1: evidence for a role in genomic RNA encapsidation. *Journal of virology* **74**: 5441-5451.

Papaleo E, Saladino G, Lambrughi M, Lindorff-Larsen K, Gervasio FL, Nussinov R. 2016. The Role of Protein Loops and Linkers in Conformational Dynamics and Allostery. *Chemical reviews* **116**: 6391-6423.

Park E, Gleghorn ML, Maquat LE. 2013. Staufen2 functions in Staufen1-mediated mRNA decay by binding to itself and its paralog and promoting UPF1 helicase but not ATPase activity. *Proc Natl Acad Sci U S A* **110**: 405-412.

Park E, Maquat LE. 2013. Staufen-mediated mRNA decay. *Wiley interdisciplinary reviews RNA* **4**: 423-435.

Peredo J, Villace P, Ortin J, de Lucas S. 2014. Human Staufen1 associates to miRNAs involved in neuronal cell differentiation and is required for correct dendritic formation. *PloS one* **9**: e113704.

Downloaded from rnajournal.cshlp.org on December 20, 2019 - Published by Cold Spring Harbor Laboratory Press

Ramasamy S, Wang H, Quach HN, Sampath K. 2006. Zebrafish Staufen1 and Staufen2 are required for the survival and migration of primordial germ cells. *Developmental biology* **292**: 393-406.

Rambo RP. 2017. Considerations for Sample Preparation Using Size-Exclusion Chromatography for Home and Synchrotron Sources. *Adv Exp Med Biol* **1009**: 31-45.

Ramos A, Bayer P, Varani G. 1999. Determination of the structure of the RNA complex of a double-stranded RNA-binding domain from Drosophila Staufen protein. *Biopolymers* **52**: 181-196.

Ramos A, Grunert S, Adams J, Micklem DR, Proctor MR, Freund S, Bycroft M, St Johnston D, Varani G. 2000. RNA recognition by a Staufen double-stranded RNA-binding domain. *The EMBO journal* **19**: 997-1009.

Ravel-Chapuis A, Belanger G, Yadava RS, Mahadevan MS, DesGroseillers L, Cote J, Jasmin BJ. 2012. The RNA-binding protein Staufen1 is increased in DM1 skeletal muscle and promotes alternative pre-mRNA splicing. *The Journal of cell biology* **196**: 699-712.

Ravel-Chapuis A, Crawford TE, Blais-Crepeau ML, Belanger G, Richer CT, Jasmin BJ. 2014. The RNA-binding protein Staufen1 impairs myogenic differentiation via a c-myc-dependent mechanism. *Molecular biology of the cell* **25**: 3765-3778.

Ravel-Chapuis A, Klein Gunnewiek A, Belanger G, Crawford Parks TE, Cote J, Jasmin BJ. 2016. Staufen1 impairs stress granule formation in skeletal muscle cells from myotonic dystrophy type 1 patients. *Molecular biology of the cell* **27**: 1728-1739.

Ricci EP, Kucukural A, Cenik C, Mercier BC, Singh G, Heyer EE, Ashar-Patel A, Peng L, Moore MJ. 2014. Staufen1 senses overall transcript secondary structure to regulate translation. *Nature structural & molecular biology* **21**: 26-35.

Rigbolt KT, Prokhorova TA, Akimov V, Henningsen J, Johansen PT, Kratchmarova I, Kassem M, Mann M, Olsen JV, Blagoev B. 2011. System-wide temporal characterization of the proteome and phosphoproteome of human embryonic stem cell differentiation. *Sci Signal* **4**: rs3.

Schupbach T, Wieschaus E. 1986. Germline autonomy of maternal-effect mutations altering the embryonic body pattern of Drosophila. *Developmental biology* **113**: 443-448.

St Johnston D, Beuchle D, Nusslein-Volhard C. 1991. Staufen, a gene required to localize maternal RNAs in the Drosophila egg. *Cell* **66**: 51-63.

St Johnston D, Brown NH, Gall JG, Jantsch M. 1992. A conserved double-stranded RNA-binding domain. *Proceedings of the National Academy of Sciences of the United States of America* **89**: 10979-10983.

Thomas JM, Beal PA. 2017. How do ADARs bind RNA? New protein-RNA structures illuminate substrate recognition by the RNA editing ADARs. *BioEssays : news and reviews in molecular, cellular and developmental biology* **39**.

Tria G, Mertens HD, Kachala M, Svergun DI. 2015. Advanced ensemble modelling of flexible macromolecules using X-ray solution scattering. *IUCrJ* **2**: 207-217.

Tria G, Mertens, H. D. T., Kachala, M. & Svergun, D. I. 2015. Advanced ensemble modelling of flexible macromolecules using X-ray solution scattering. *IUCrJ* **2**: 207-217.

Tsutakawa SE, Lafrance-Vanasse J, Tainer JA. 2014. The cutting edges in DNA repair, licensing, and fidelity: DNA and RNA repair nucleases sculpt DNA to measure twice, cut once. *DNA Repair (Amst)* **19**: 95-107.

Vessey JP, Macchi P, Stein JM, Mikl M, Hawker KN, Vogelsang P, Wieczorek K, Vendra G, Riefler J, Tubing F et al. 2008. A loss of function allele for murine Staufen1 leads to impairment of dendritic Staufen1-RNP delivery and dendritic spine morphogenesis.

Downloaded from rnajournal.cshlp.org on December 20, 2019 - Published by Cold Spring Harbor Laboratory Press

Proceedings of the National Academy of Sciences of the United States of America **105**: 16374-16379.

Vranken WF, Boucher W, Stevens TJ, Fogh RH, Pajon A, Llinas M, Ulrich EL, Markley JL, Ionides J, Laue ED. 2005. The CCPN data model for NMR spectroscopy: development of a software pipeline. *Proteins* **59**: 687-696.

Wang X, Vukovic L, Koh HR, Schulten K, Myong S. 2015. Dynamic profiling of double-stranded RNA binding proteins. *Nucleic acids research* **43**: 7566-7576.

Weigelt J. 1998. Single Scan, Sensitivity- and Gradient-Enhanced TROSY for Multidimensional NMR Experiments. *J Am Chem Soc* **120**: 10778−10779.

Wickham L, Duchaine T, Luo M, Nabi IR, DesGroseillers L. 1999. Mammalian staufen is a double-stranded-RNA- and tubulin-binding protein which localizes to the rough endoplasmic reticulum. *Molecular and cellular biology* **19**: 2220-2230.

Zhou H, Di Palma S, Preisinger C, Peng M, Polat AN, Heck AJ, Mohammed S. 2013. Toward a comprehensive characterization of a human cancer cell phosphoproteome. *J Proteome Res* **12**: 260-271.

Downloaded from rnajournal.cshlp.org on December 20, 2019 - Published by Cold Spring Harbor Laboratory Press

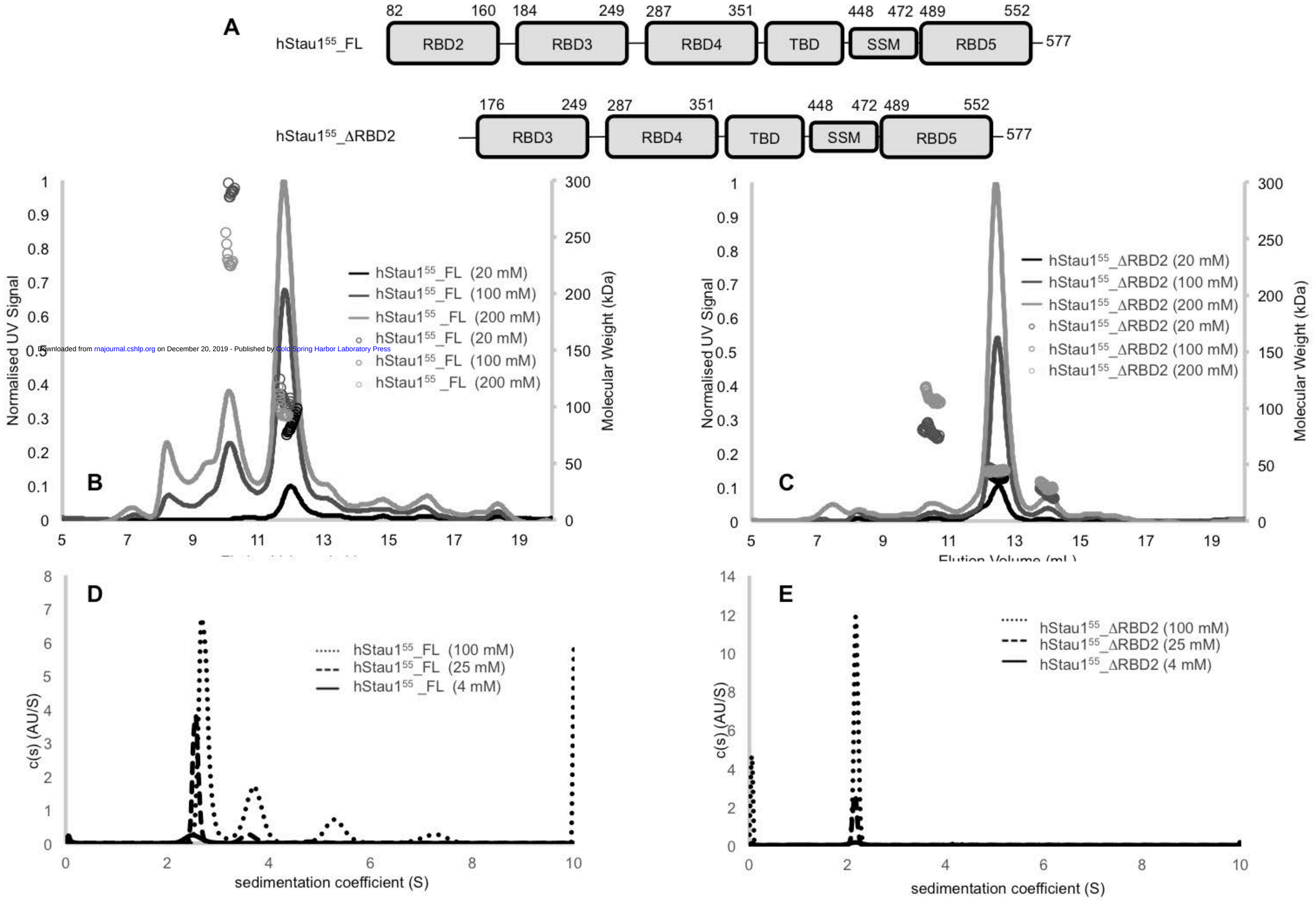

Figure 1: **Architecture and biophysical characterization of Staufen proteins.** A: Domains organization of hStau1^{55}_FL and hStau1^{55}_ΔRBD2. B: SEC-MALS of hStau1^{55}_FL at 20,100 and 200 µM. C: SEC-MALS of hStau1^{55}_ΔRBD2 at 20,100 and 200 µM. D: Analytical ultracentrifugation (AUC) of hStau1^{55}_FL at 4, 25 and 100 µM. E: Analytical ultracentrifugation (AUC) of hStau1^{55}_ΔRBD2 at 4, 25 and 100 µM.

Figure 2

Downloaded from rnajournal.cshlp.org on December 20, 2019 - Published by Cold Spring Harbor Laboratory Press

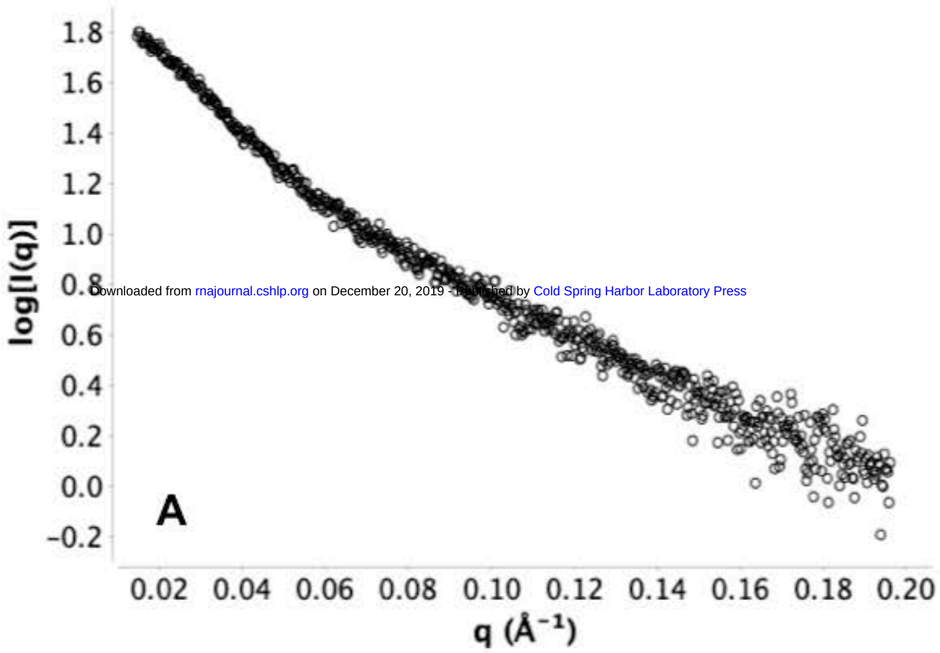

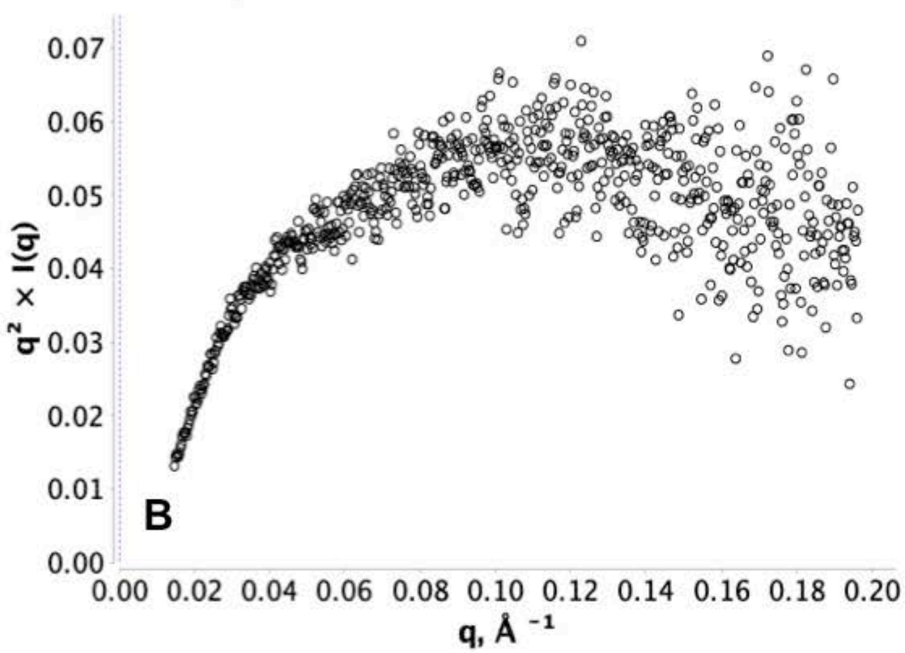

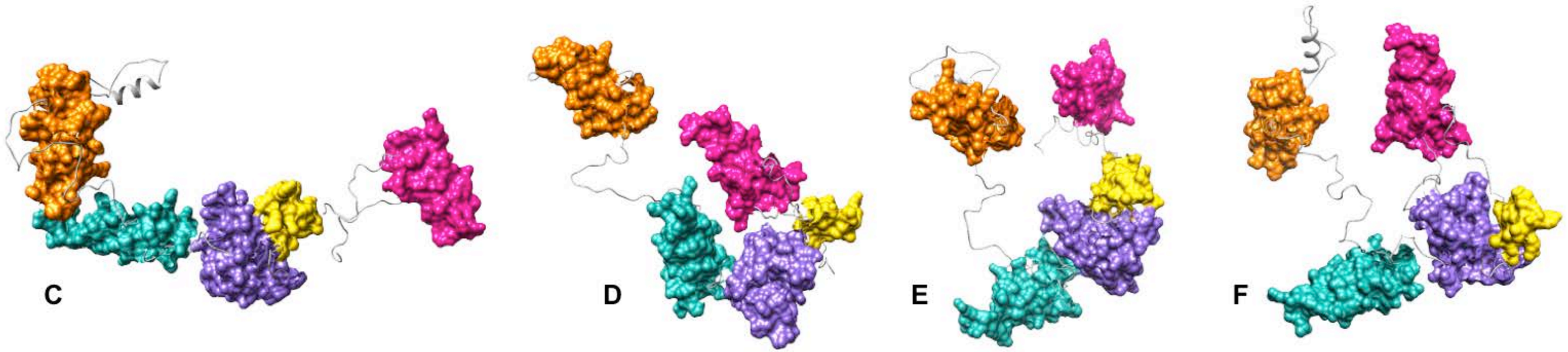

Domains: RBD3, RBD4, TBD, SSM, RBD5.

Figure 2: **Small angle X-ray scattering (SAXS) of Staufen proteins.** A: SAXS intensity curve; B. Kratky analysis; C-F. EOM models generated for hStau1^{55}_ΔRBD2 at 60 µM [R_g *ensemble*= 50.26 Å, D_{max} *ensemble*= 166.96 Å, R_{sigma}= ~80.2% (~85.68%)].

Figure 3

Downloaded from rnajournal.cshlp.org on December 20, 2019 - Published by Cold Spring Harbor Laboratory Press

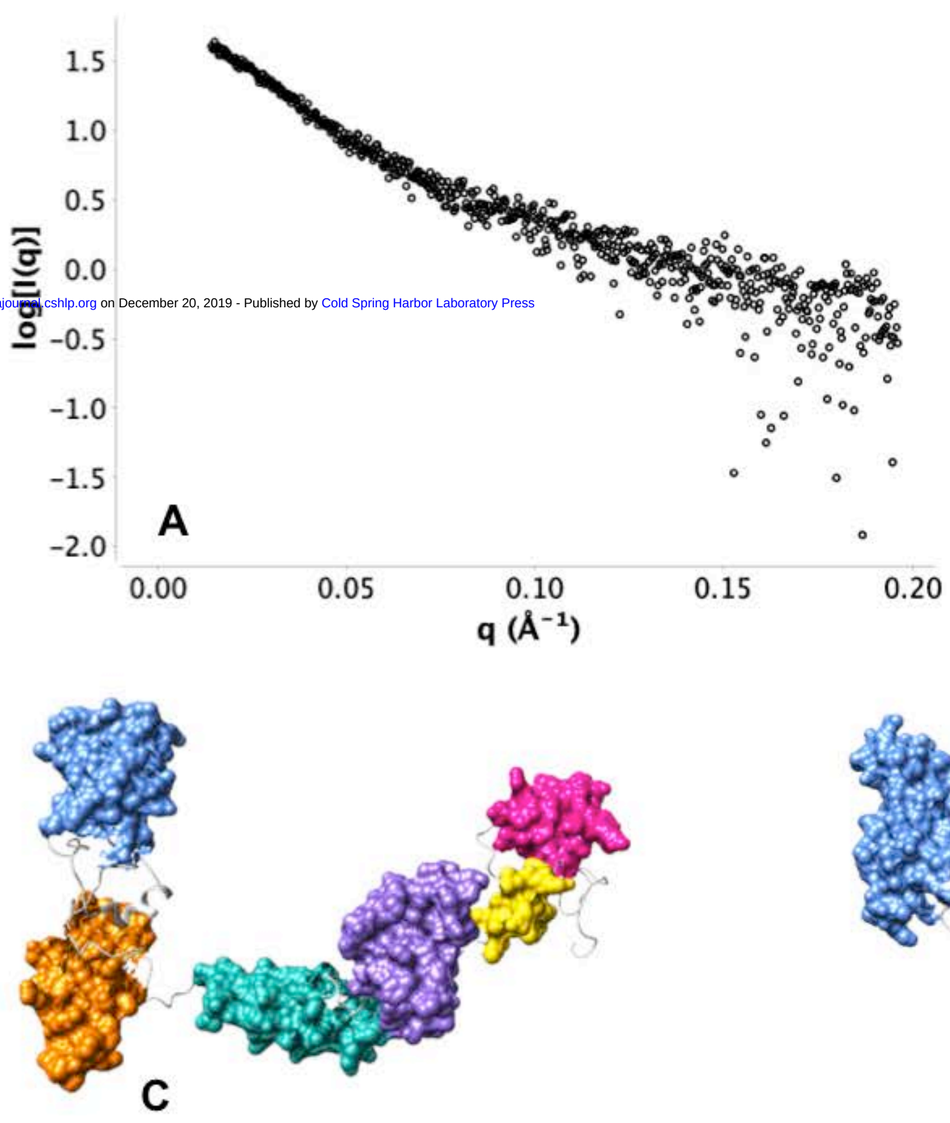

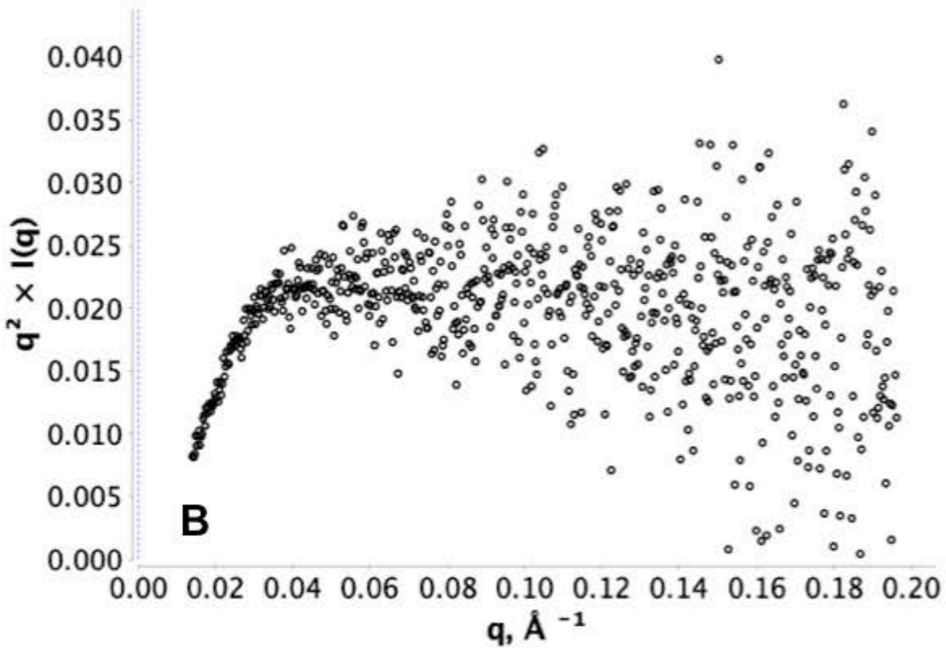

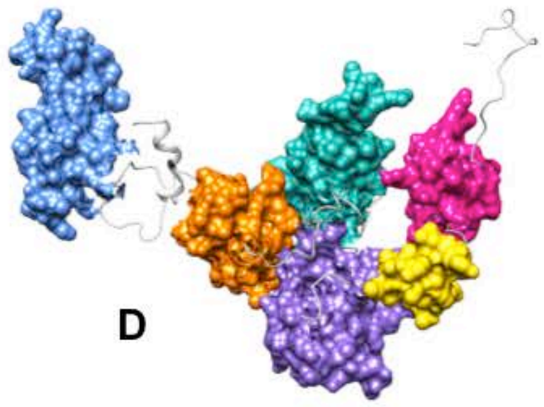

Domains: RBD2, RBD3, RBD4, TBD, SSM, RBD5.

Figure 3: Small angle X-ray scattering (SAXS) of Staufen proteins. A: SAXS intensity curve; B. Kratky analysis; C-E. EOM models generated for hStau1^{55}_FL at 40 μM [R_g *ensemble*= 48.11 Å, D_{max} *ensemble*= 155.2 Å, R_{sigma}= ~74.45% (~86.17%)].

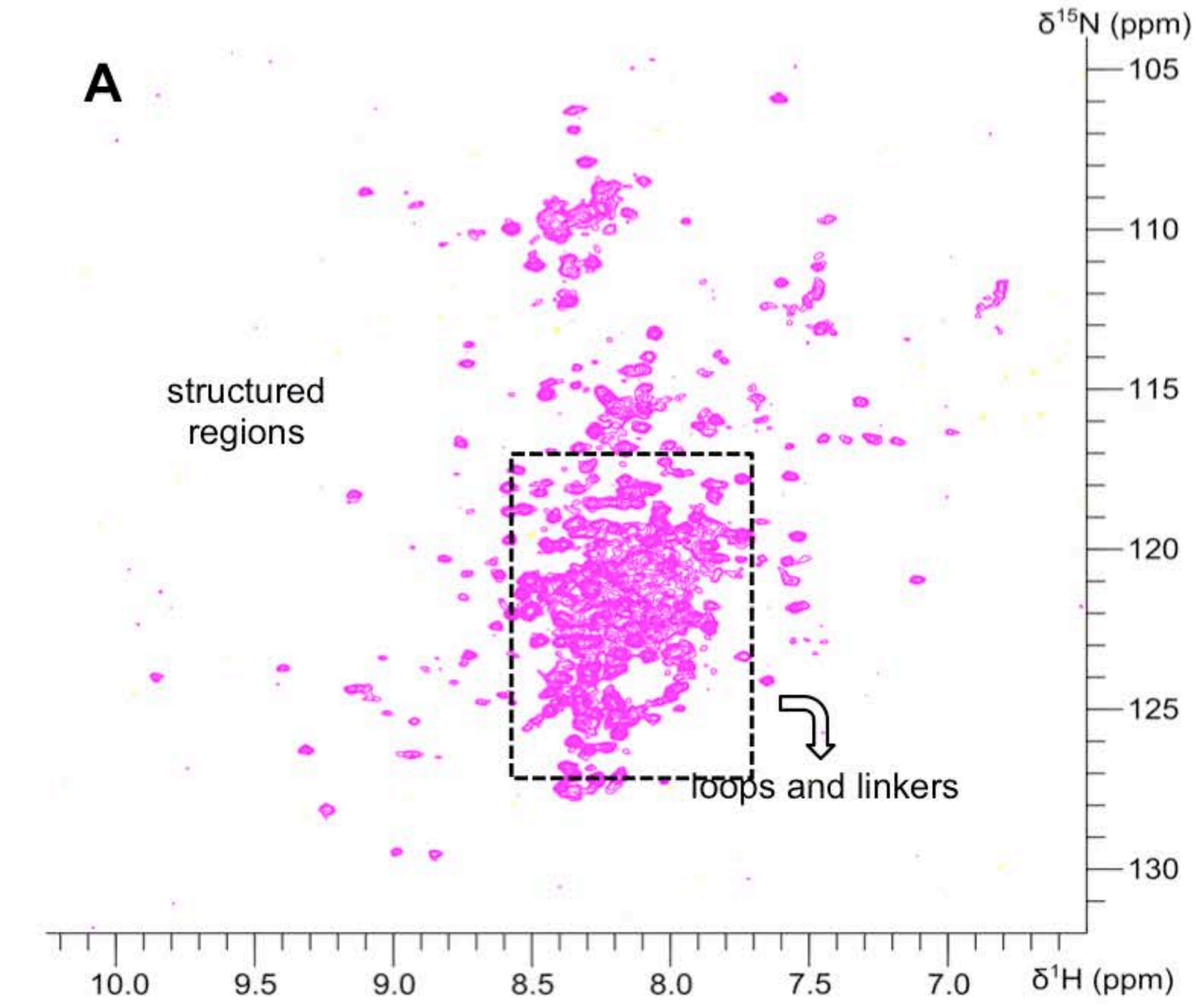

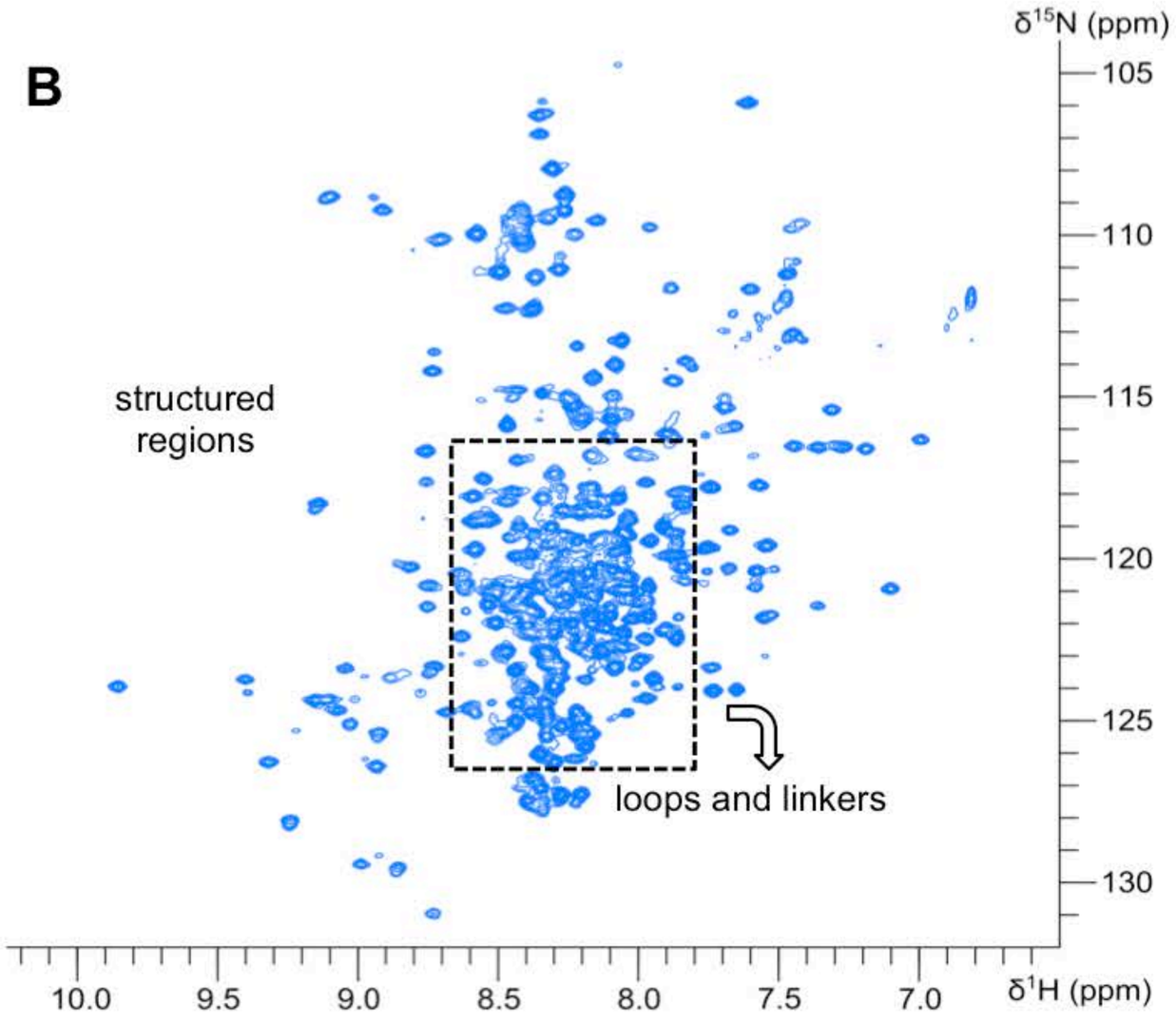

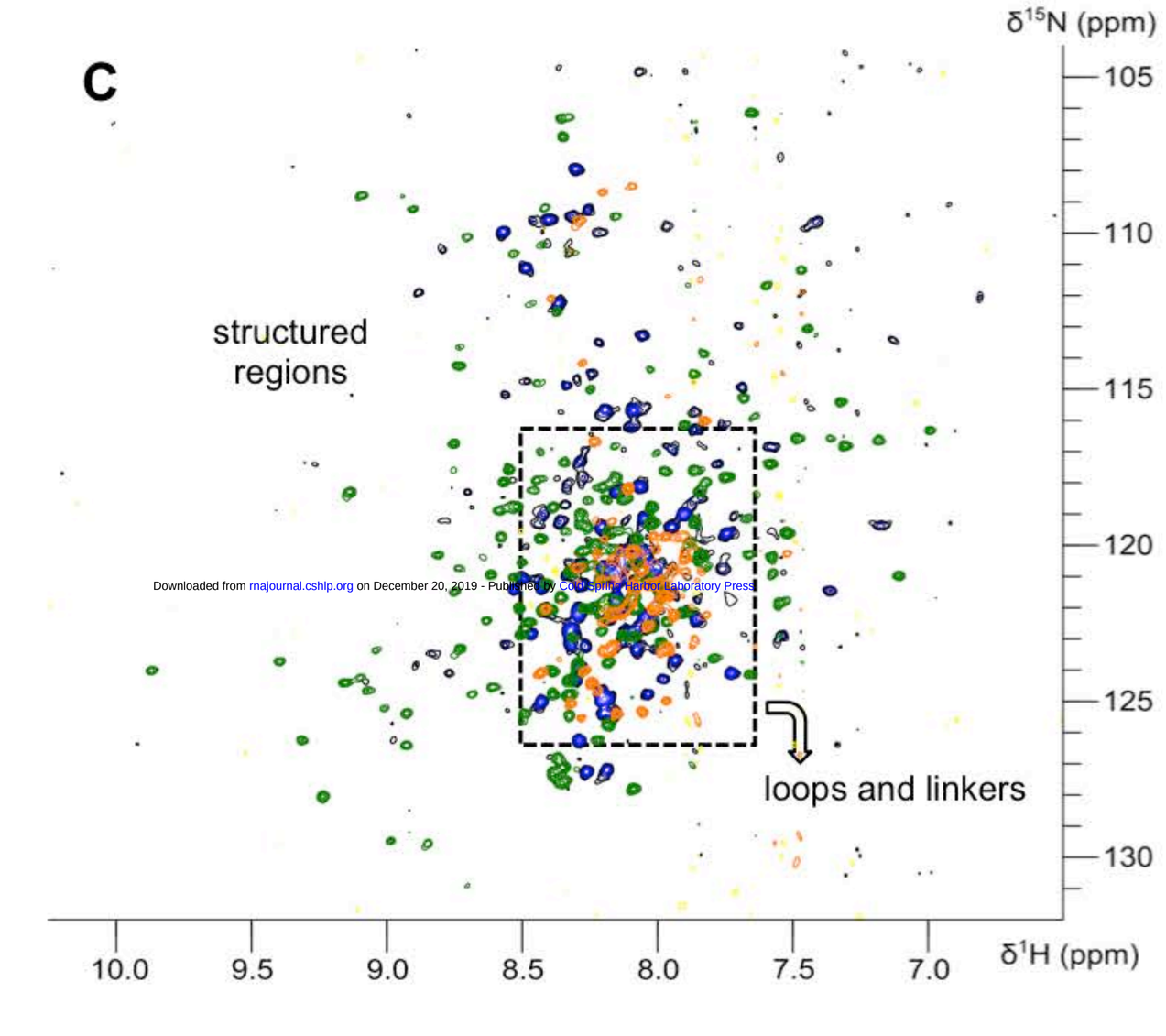

Downloaded from rnajournal.cshlp.org on December 20, 2019 - Published by Cold Spring Harbor Laboratory Press

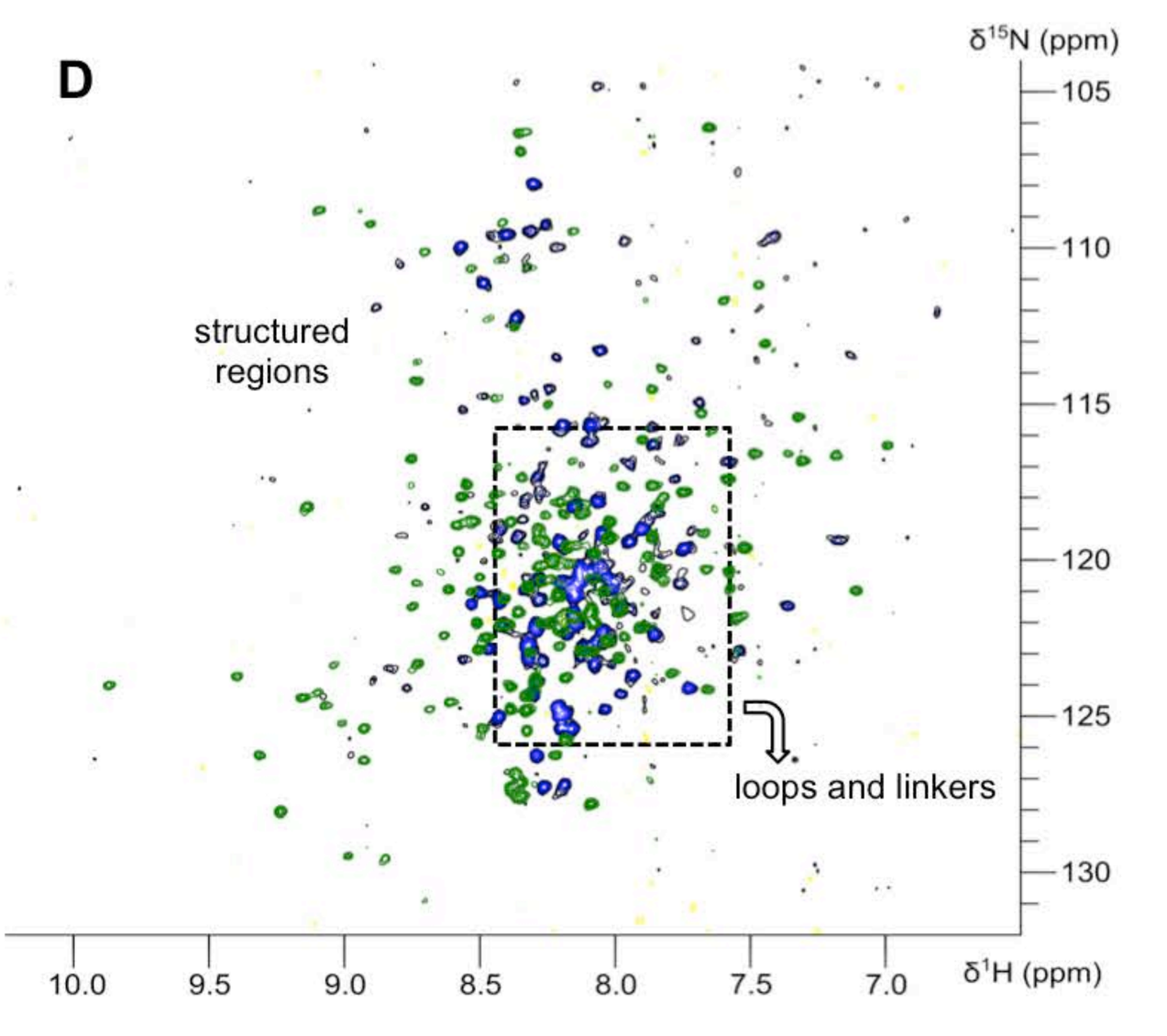

Figure 4: **NMR of Staufen proteins.** A: NMR spectra of hStau1^{55}_FL. B: NMR spectra of hStau1^{55}_DRBD2. C: Reconstitution of hStau1^{55}_FL spectra by overlapping of RBD2, RBD3-RBD4 and TBD-SSM/RBD5 NMR spectra. D: Reconstitution of hStau1^{55}_ DRBD2 spectra by overlapping of RBD2, RBD3-RBD4 and TBD-SSM/RBD5 NMR spectra.

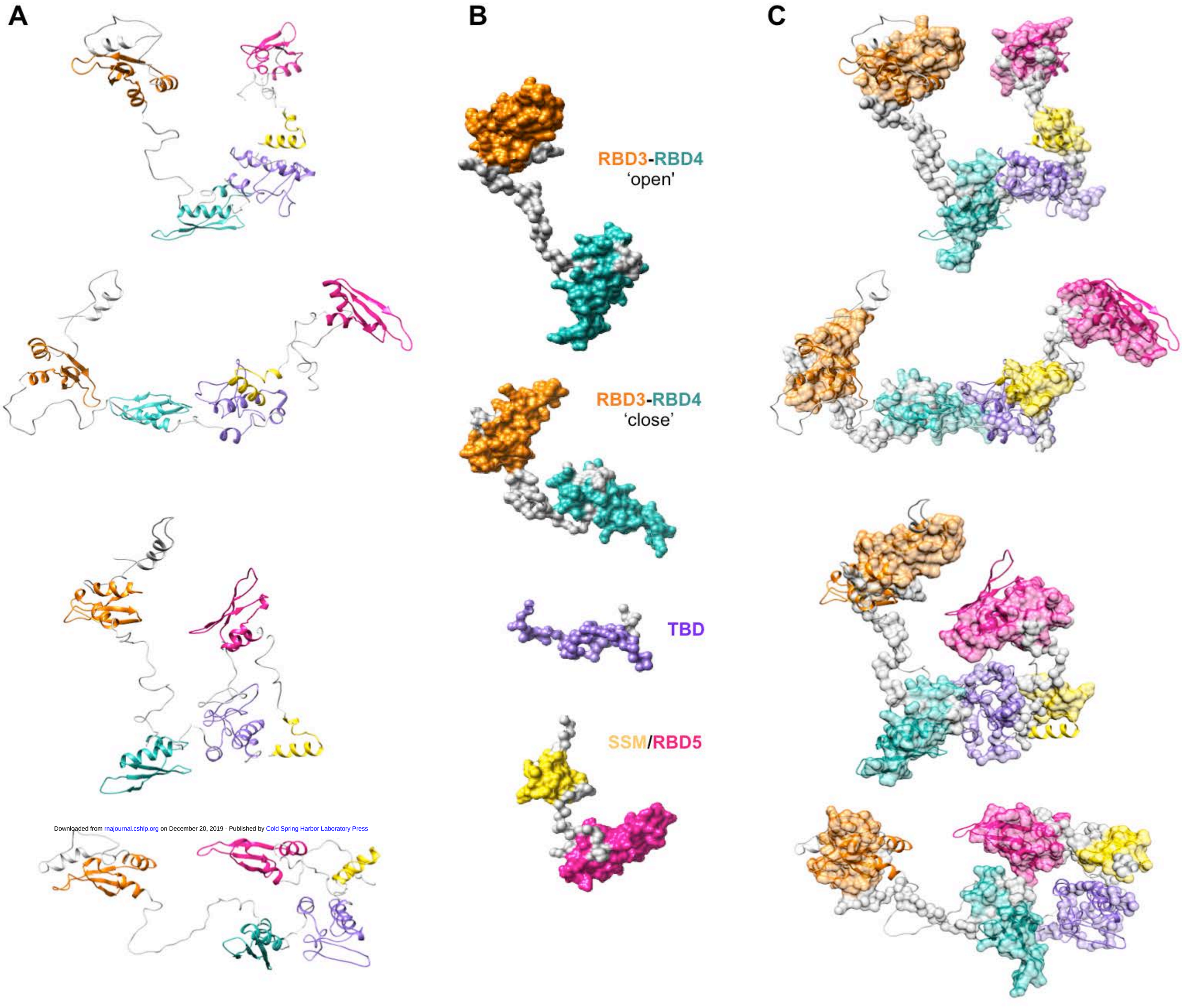

Downloaded from rnajournal.cshlp.org on December 20, 2019 - Published by Cold Spring Harbor Laboratory Press

Figure 5. **Fitting of SAXS models for Staufen1 domains in the SAXS models obtained for hStau1^{55}_DRBD2.** A: EOM models generated for hStau1^{55}_DRBD2. B: Subset of selected domains and tandem domains models. C: Fitting of representative models for domains and tandem domains in the EOM models generated for hStau1^{55}_DRBD2.

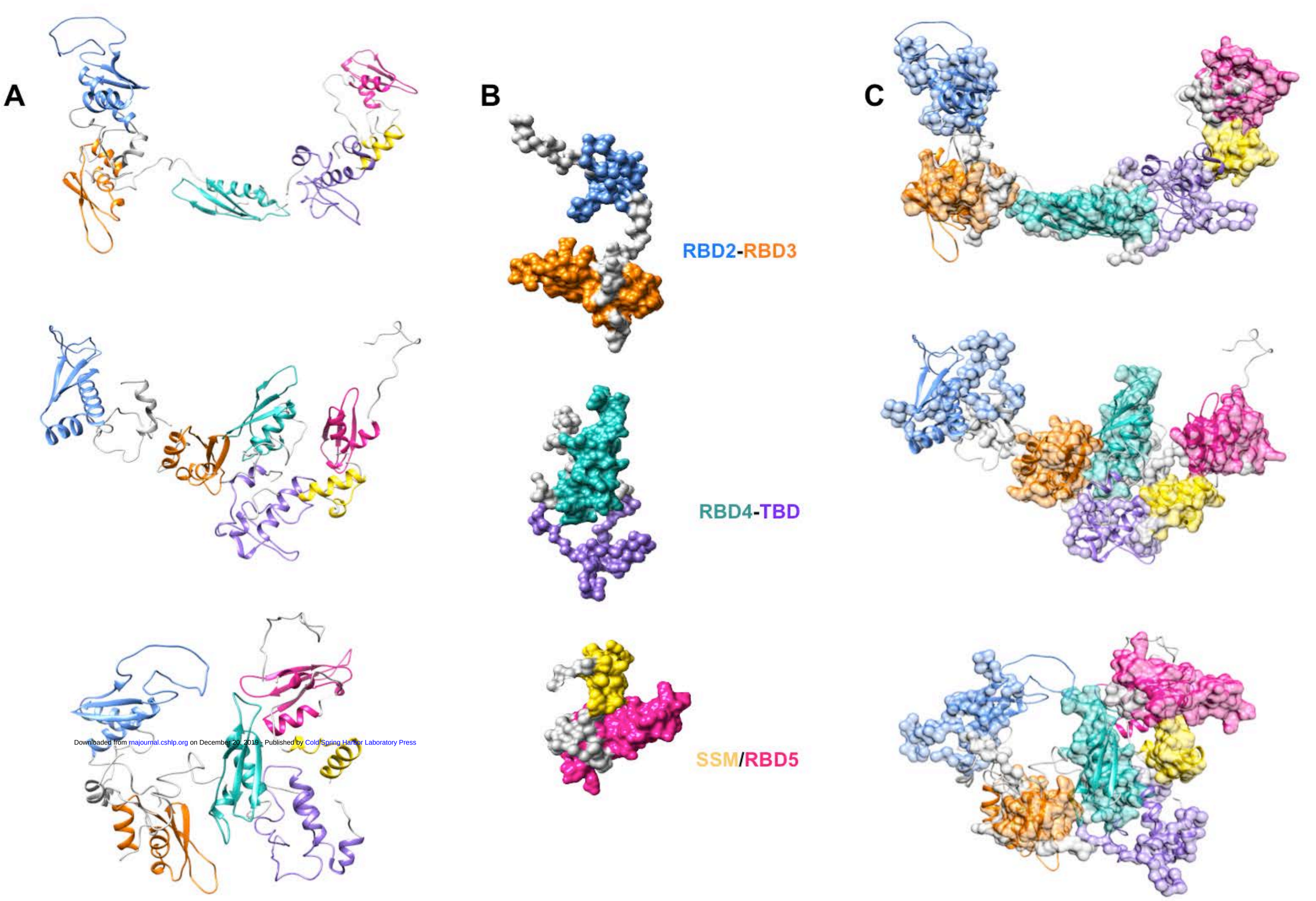

Downloaded from rnajournal.cshlp.org on December 20, 2019 - Published by Cold Spring Harbor Laboratory Press

Figure 6. **Fitting of SAXS models for Staufen1 domains in the SAXS models obtained for hStau1^{55}_FL.** A: EOM models generated for hStau1^{55}_FL. B: Subset of selected domains and tandem domains models. C: Fitting of representative models for domains and tandem domains in the EOM models generated for hStau1^{55}_FL.

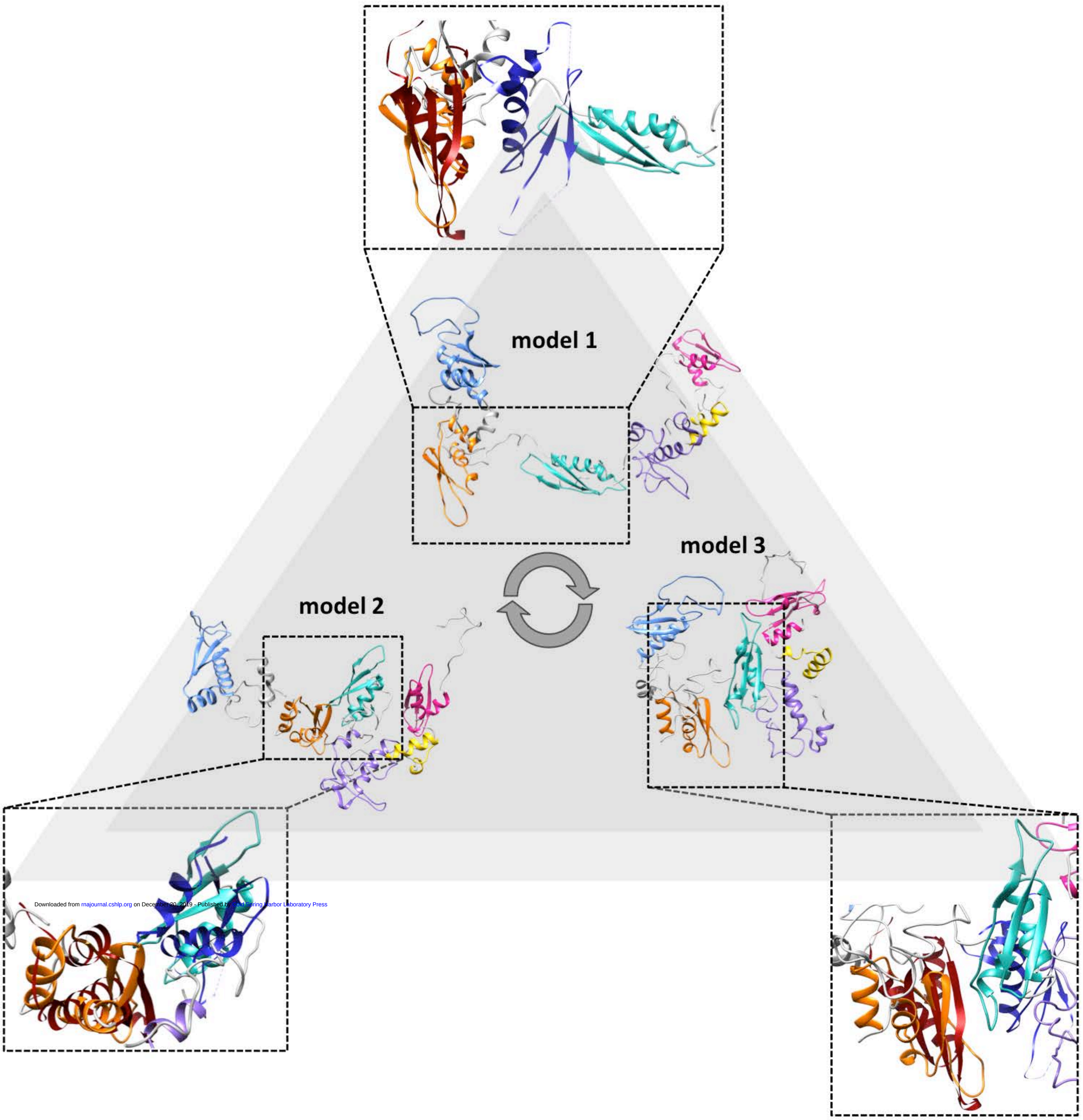

Downloaded from rnajournal.cshlp.org on December 20, 2019 - Published by Cold Spring Harbor Laboratory Press

Figure 7. **RBD3 and RBD4 rearrangements in hStau1^{55}_FL can explain its plasticity in the binding of diverse dsRNA targets.** The SAXS models obtained for hStau1^{55}_FL show that RBD3 (orange) and RBD4 (cyan) transit from a 'open' to a 'more closed' conformation. A direct comparison of our models with the crystal structure of the hStau1^{63} RBD3-RBD4 construct bound to Arf1 SBS[43] (RBD3 displayed in red and RBD 4 in blue) shows that RBD3 and RBD4 are 'pulled' towards each other by conformational changes of the connecting linker, possibly in order to elicit dsRNA binding.

Downloaded from rnajournal.cshlp.org on December 20, 2019 - Published by Cold Spring Harbor Laboratory Press

A multi-pronged approach to understanding the form and function of hStaufen protein

Silvia Visentin, Giuseppe Cannone, James Doutch, et al.

RNA published online December 18, 2019

Supplemental Material http://rnajournal.cshlp.org/content/suppl/2019/12/18/rna.072595.119.DC1

P<P Published online December 18, 2019 in advance of the print journal.

Accepted Manuscript Peer-reviewed and accepted for publication but not copyedited or typeset; accepted manuscript is likely to differ from the final, published version.

Creative Commons License This article is distributed exclusively by the RNA Society for the first 12 months after the full-issue publication date (see http://rnajournal.cshlp.org/site/misc/terms.xhtml). After 12 months, it is available under a Creative Commons License (Attribution-NonCommercial 4.0 International), as described at http://creativecommons.org/licenses/by-nc/4.0/.

Email Alerting Service Receive free email alerts when new articles cite this article - sign up in the box at the top right corner of the article or **click here.**

To subscribe to *RNA* go to:
http://rnajournal.cshlp.org/subscriptions

Published by Cold Spring Harbor Laboratory Press for the RNA Society